Nanoscale

PAPER

View Article Online
View Journal | View Issue

Cite this: *Nanoscale*, 2016, **8**, 7137

Spectra-selective PbS quantum dot infrared photodetectors

Keke Qiao,[a] Hui Deng,[a] Xiaokun Yang,[a] Dongdong Dong,[a] Min Li,[b] Long Hu,[a] Huan Liu,[b] Haisheng Song*[a] and Jiang Tang*[a]

Received 21st December 2015,
Accepted 26th February 2016

DOI: 10.1039/c5nr09069e

www.rsc.org/nanoscale

Traditional photoconductive photodetectors (PDs) commonly respond to higher energy photons compared with the bandgaps of PD active materials. Different from the wide detection spectra of traditional PDs, the present reported PbS quantum dot (QD) PDs can detect the spectra-selective light source. Spectra-selective PDs (ss-PDs) of perovskite/QDs and QD/QDs were respectively implemented by integrating two functional layers. The top layer (facing the light) was utilized to filter the non-target spectra and the bottom layer was used for detection. The response spectrum wavelength and the range of ss-PDs can be conveniently tailored by tuning the QD size. The obtained selectivity factor and normalized detectivity ratio from target and non-target illumination can reach at least 10. A narrow detection range with a full width at half maximum (FWHM) ~100 nm was applied by typical QD/QD based ss-PDs. The prototype ss-PDs were successfully applied in identifying an unknown light source. The convenient tuning and identification capabilities of the present QD based ss-PDs may provide a versatile route to obtain highly spectrum-selective PDs in order to meet the demands for special fields.

Introduction

Colloidal quantum dots (CQDs) have been recognized as an advantageous optical sensitive material over bulk and quantum well counterparts.[1–4] By virtue of the colloidal and 3D quantum confinement effect, QDs possess solution-process operability, compatible with common substrates and a size-tunable detection wavelength,[5,6] which promises wide applications in various kinds of optoelectronic devices.[7–9] PbS CQDs not only inherit the characters of common QDs but also hold their own advantages such as large Bohr exciton radii (~18 nm),[10] high transport mobilities,[11] easy and reliable synthesis process and wide absorption range (UV to IR).[12] PbS CQD based optoelectronics have developed very quickly over the last two decades. Up to now, PbS QD solar cells have got a certified efficiency of 10% by ligand and interface engineering.[13,14] Photoconductive IR detectors[15] obtained a normalized detectivity of $\sim 1.8 \times 10^{13}$ Jones working at room temperature, which is one order higher than commercial silicon PDs.[2] For the detection spectra of PbS QD photoconductive PDs, they show a broad response range due to their small bandgaps. However, the non-target spectra introduce the additional noise and might lead to a series of deteriorated effects such as lower resolution, sensitivity, reliability *etc.*[12,15] Therefore, spectra-selective PDs (ss-PDs) of PbS QDs are designed and expected to avoid the above problems to suit special application fields.

To obtain photoconductive ss-PDs, there are mainly two types of techniques to tailor the response spectra of PDs. One is epitaxial growth[16,17] or the deposition of a larger bandgap semiconductor atop the active layer[18] which worked to eliminate the short-wavelength photons. The other is tuning the semiconductor alloy compositions to match the selective response spectra.[19,20] Inorganic film ss-PDs have exhibited ultra-narrow spectra and high responsivity in the UV[16,17] and visible range.[19] However, the traditional inorganic bulk semiconductors hold challenges to tune the absorption range due to the fixed bandgaps. In contrast, for PbS QDs, the quantum size effect makes it very convenient to tune the light response. And the solution processing is compatible with the mature semiconductor device fabrication techniques. Therefore, the present work utilized PbS CQDs to investigate the ss-PDs.

For IR ss-PDs, the extinction to UV and visible spectra was the basic requirement for the top layer of ss-PDs. It is well known that organolead triiodide perovskite (OTP) is an excellent absorption material with a high light absorption coefficient ($>10^5$ cm^{-1}) at the visible range,[21] a suitable bandgap (~1.55 eV)[22] and a compatible fabrication procedure as QD PDs. Thus OTP was a perfect material as the top layer to eliminate the non-target spectra.

[a]*Wuhan National Laboratory for Optoelectronics (WNLO), Huazhong University of Science and Technology (HUST), 1037 Luoyu Road, Wuhan, Hubei 430074, China. E-mail: songhs-wnlo@mail.hust.edu.cn, jtang@mail.hust.edu.cn*
[b]*School of Optical and Electronic Information, Huazhong University of Science and Technology (HUST), 1037 Luoyu Road, Wuhan, Hubei 430074, China*

Herein, two types of ss-PDs with perovskite/PbS QD and QD/QD device structures were designed and implemented by stacking two functional layers. A series of prototype devices verified the selective detection capabilities and narrowed the response spectra with a full width at half maximum (FWHM) of about 100 nm. The combination of three developed PDs successfully recognized an unknown IR input. The presented ss-PDs with a high sensitivity and narrow response range are expected to be applied in special application fields such as spectroscopy, confidential communications, security switches and so on.

Results and discussion

Traditional photoconductive PbS QD PDs

First of all, traditional PbS QD PDs composed of one layer of QDs from the same batch were fabricated to investigate the PD selectivity. The as-synthesized PbS QDs with the first exciton absorption peak located at 980 nm is shown in Fig. 1a. It was noted that, if not specified, PbS QDs were denoted by their wavelengths of the first exciton absorption peaks. And the size of PbS QDs was about 3.2 nm according to Moreels equation.[23] The peak to valley ratio was ~3 demonstrating uniform QD size distribution.[24] The PD responses to varied wavelengths of monochromatic light are shown in Fig. 1b. The photocurrent increased gradually from about 3 nA to 6 nA as the light wavelength increased from 390 nm to 930 nm. Once the illumination light exceeded its absorption range such as 1200 nm light, the photocurrent sharply decreased to about 1.1 nA similar to the dark current.

For a photoconductive PDs, switching ratio (SR), responsivity (R) and detectivity (D^*) are the figures of merit to characterize the PD performance of different devices. The PD switching ratio was calculated by SR = I_p/I_d = $(I_{on} - I_d)/I_d$; responsivity shows device sensitivity toward light detection calculated from $R = \frac{I_p}{P}$; and for the photoconductive PD, the shot noise derived normalized detectivity can be calculated by $D^* = \frac{I_p\sqrt{A}}{P\sqrt{2qI_d}}$,[25] where I_p is the photocurrent, I_{on} is the light current, I_d is the dark current, P denotes the light power density illuminated on the device, and A is the device area; q represents the elementary charge. As the illumination wavelength increased from 390 nm to 930 nm, the responsivity and detectivity increased from 8.2 mA W^{-1} and 7.2 × 10^{10} Jones to 15.6 mA W^{-1} and 1.3 × 10^{11} Jones, respectively. Once the input wavelength exceeded the QD band edge such as 1200 nm, the responsivity and detectivity both decreased rapidly similar to a dark signal without response. Therefore, the response of traditional PDs confirmed the shorter wavelength photon response compared with its absorption band edge. In order to implement selective detection, the non-target spectra should be eliminated by depositing a top layer.[16,18]

OTP/PbS QD ss-PDs

The first type of ss-PDs was made of an OTP top layer and PbS QDs' bottom layer, which is simplified as OTP/PbS ss-PDs. And three typical size QDs were utilized to tailor the response spectrum range. Their first exciton absorption peaks were located at 780 nm, 1060 nm and 1390 nm, respectively (Fig. 2a). All the XRD peaks (Fig. 2b) were in accordance with the PbS standard PDF card (JCPDS no: 02-0699). The 1390 nm QDs were selected to be further characterized by HRTEM as shown in Fig. 2c. And the QD size was about 5 nm consistent with UV-vis spectra calculation results. From the HRTEM image, the QD sizes were uniform and each was isolated by ligand passivation. Fig. 3a shows the morphologies of the top OTP layer with a smooth and compact surface and the grain size was about 200–300 nm. The XRD spectra confirmed the OTP phase and was consistent with the spectra reported in the literature.[26,27] The strong peak intensity and narrow FWHM of XRD spectra manifested the high quality of the OTP film.

The device structure and cross section SEM image are shown in Fig. 4a. The inter-layer, poly(methyl methacrylate) (PMMA) between the OTP and PbS layer was adopted to avoid the top layer signal affection and blind to IR spectra. Fig. 4b–d show the illumination dependent ss-PD responses. All the devices had the same device structure of OTP/PMMA/PbS

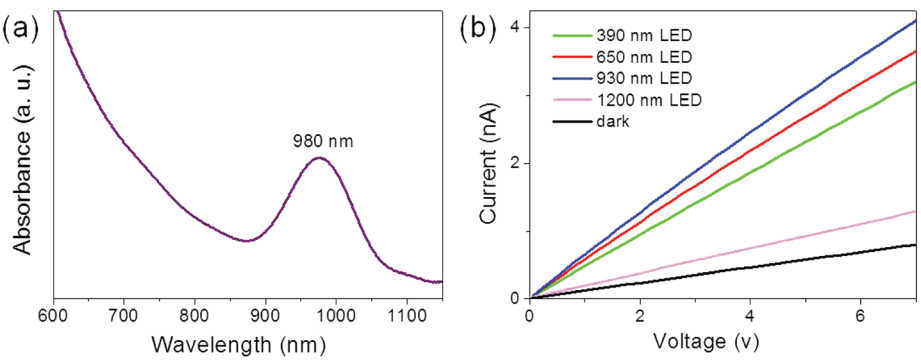

Fig. 1 Characterization of a traditional photoconductive PbS QD detector. (a) PbS QDs with the first exciton absorption peak located at 980 nm; (b) current–voltage (I–V) curves of the same one 980 nm PbS QD PD in the dark and under various LED light (390 nm, 650 nm, 930 nm and 1200 nm) illuminations with the same power intensity (20 μW cm^{-2}). The bias voltage is all at 10 V.

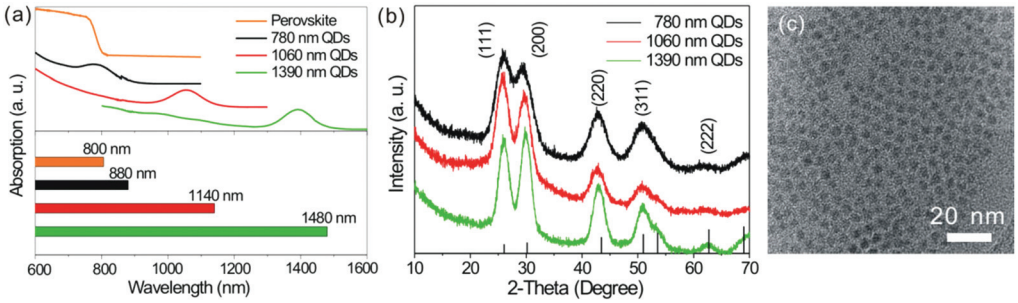

Fig. 2 (a) Top: absorption of perovskite (orange) and three kinds of PbS QDs with different first exciton absorption peaks: 780 nm (black), 1060 nm (red), 1390 nm (green). Bottom: the bar charts in different color for the absorption range and the onset absorption wavelength. (b) XRD spectra of 780 nm, 1060 nm, 1390 nm PbS QDs. (c) HRTEM image of 1390 nm PbS QDs.

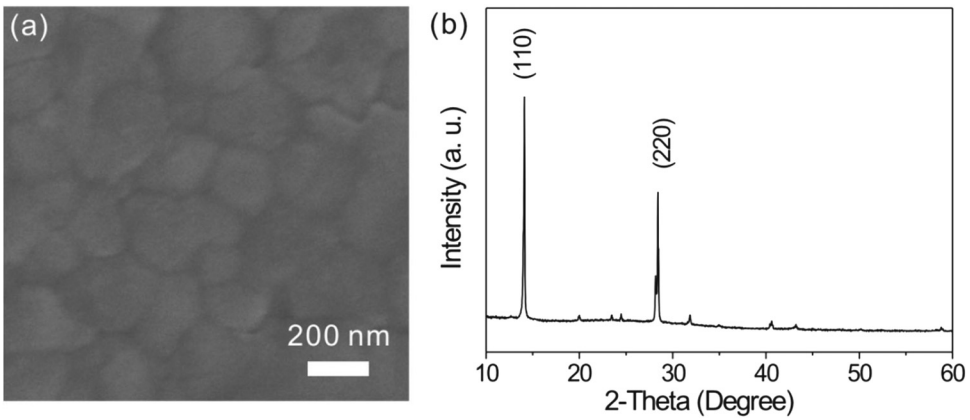

Fig. 3 Characterization of the prepared OTP ($CH_3NH_3PbI_3$) film: (a) smooth and compact OTP film with grain size ~200 nm; (b) XRD diffraction of perovskite.

QD/glass ss-PDs and the only difference was the first exciton absorption peak of the bottom layer. They were 780 nm, 1060 nm and 1390 nm QDs corresponding to Fig. 4b–d, respectively. The inset of each figure schematically described the device components in different colors. The stacking layers in orange, black, red and green denoted the OTP, 780 nm QDs, 1060 nm QDs and 1390 nm QDs, respectively. Each device was respectively tested by target light and non-target light to manifest the selective detection capability. The target light was from the onset absorption wavelength of the bottom layer to the onset one of the top layer. Fig. 4b shows distinct *I–t* responses under 650 nm (non-target spectrum) and 1400 nm (target spectrum) light illuminations. All the on-state currents were normalized to their own dark current for convenient comparison. And the PD SRs were 0.13 and 3 from 650 nm and 1400 nm light excitation, respectively. A new term, selectivity factor, was defined as $(SR)_T/(SR)_N$ in order to judge the selective detection capability of present PDs, where T and N denoted the signals obtained from target spectrum illumination and non-target spectrum excitation, respectively. The respective selectivity factors for Fig. 4b–d reached 30, 20 and 10. Under the same measuring conditions, all the target signals were at least one order higher than non-target spectrum signals only by changing the illumination wavelength. Another new term was the normalized detectivity ratio which is defined by $(D^*)_T/(D^*)_N$. According to the above definition, the normalized detectivity ratios as shown in Fig. 4b–d reached 30, 10 and 40, respectively. Both the target selectivity factors and the detectivity ratios reached one order higher than the signals from non-target spectrum illumination. Therefore, the OTP/PbS QD ss-PDs can indeed selectively detect various IR wavelength inputs.

The working mechanism of the present ss-PDs was explained from combining the absorption properties of the stacking layers. The top layer diminished the spectra from onset absorption (λ_1); on the other hand, the bottom layer could only respond to the spectrum shorter than its onset absorption (λ_2). By stacking the above two layers for detection, efficient detection spectra was expected to start from λ_1 to λ_2. It can be inferred that the selective range of the spectra of OTP/1390 nm ss-PDs (Fig. 4b) was about 800 nm–1480 nm. And the detection ranges of OTP/1060 nm (Fig. 4c) and OTP/780 nm (Fig. 4d) ss-PDs were about 800 nm–1140 nm and 800 nm–880 nm, respectively. By utilizing smaller QDs as the bottom layer, the selective spectra were tuned and narrowed from 800 nm–1480 nm to 800 nm–880 nm.

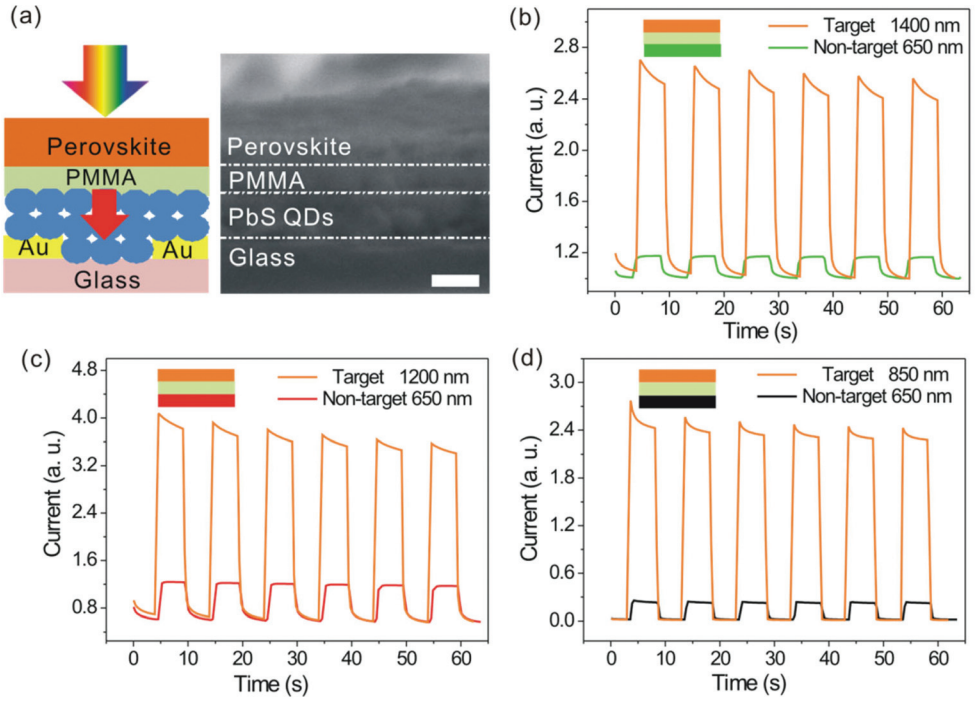

Fig. 4 Performances of OTP/PbS QD ss-PDs. (a) Schematic diagram and cross-section SEM image of glass/PbS QD/PMMA/OTP ss-PDs. The scale bar is 200 nm. (b–d) Normalized *I*–*t* curves of OTP/1390 nm (b), OTP/1060 nm (c) and OTP/780 nm (d) QD ss-PDs which were respectively obtained from multi-cycles of target and non-target LED light illumination. Insets of b–d show the stacking layers of the device compositions in different colors. The orange, black, red and green layers denote the OTP, 780 nm QDs, 1060 nm QDs and 1390 nm QDs, respectively. All the measurements utilized 20 μW cm^{-2} power intensity and 10 V bias voltage.

The above OTP/PbS QD ss-PDs could detect the spectra from 800 nm (top OTP band edge) to the absorption band edge of the bottom QD layer. However, the starting detection spectrum was fixed due to the top OTP layer. While being different from traditional semiconductor bandgaps, the bandgaps of PbS QDs were convenient to be tuned from 2 eV to 0.5 eV by facilely manipulating the quantum size. The integration of two PbS QD layers with matched bandgaps was more convenient to further tailor the detection spectra.

S-QD/L-QD ss-PDs

Fig. 5a shows the schematic diagram of the S-QD/L-QD ss-PDs, where the S-QD (red solid circles) and the L-QD (green solid circles) denoted the small size and large size QDs, respectively. Similar to the above OTP/PbS QD ss-PDs, three types of S-QD/L-QD ss-PD prototype devices were fabricated to verify the selective detection. The corresponding exciton absorption peaks were 780 nm and 1390 nm, 780 nm and 1060 nm, 1060 nm and 1390 nm, respectively. The detection results of the three kinds of S-QD/L-QD ss-PDs excited by non-target spectra and target spectra are shown in Fig. 5b–d. The device selectivity factors and detectivity ratios were 20 and 30 (Fig. 5b), and 30 and 30 (Fig. 5c), respectively. The one order stronger signal response demonstrated the spectra-selective detection capability. The inferred device detection ranges of Fig. 5b and c were 880 nm–1480 nm and 880 nm–1140 nm, respectively. Similar to OTP/PbS QD ss-PDs, the detection range could be tuned and narrowed by changing the bottom layer QD size from 1390 nm QDs (Fig. 5b) to 1060 nm QDs (Fig. 5c). Different from OTP/PbS QD ss-PDs, 1060 nm/1390 nm ss-PDs (Fig. 5d) could simultaneously tune the top layer QD size in order to tailor the onset response spectrum. And the inferred detection ranges of Fig. 5d was evolved into 1140–1480 nm. The selectivity factor and detectivity ratio of 1060 nm/1390 nm ss-PDs reached 10 and 110, respectively. Therefore, only by tuning the QD size of the top and bottom layers, the required detection range could be facilely manipulated.

The selective detection ranges of OTP/QD (Fig. 4) and S-QD/L-QD (Fig. 5) ss-PDs were only checked by two selected spectrum (target and non-target ones) without full spectrum scanning. Typical S-QD/L-QD ss-PDs, 980 nm/1120 nm ss-PDs were scanned in full spectra to confirm our inferred results. As shown in Fig. 6a, the 980 nm/1120 nm ss-PDs only obtained responsivity from 1000 nm to 1200 nm. The selective spectra of 1000 nm–1200 nm were similar to the inferred range, which verified the credence of the inferred detection spectra of $\lambda_1 - \lambda_2$.

Recently, Lin *et al.* and Fang *et al.* have independently reported the color-selective photodetectors based on a perovskite with different components and with different structures. Lin *et al.* utilized dyes mixed with OTP as light-absorbing materials to tune the devices' external quantum efficiency by a charge collection narrowing mechanism.[28] Fang *et al.* applied

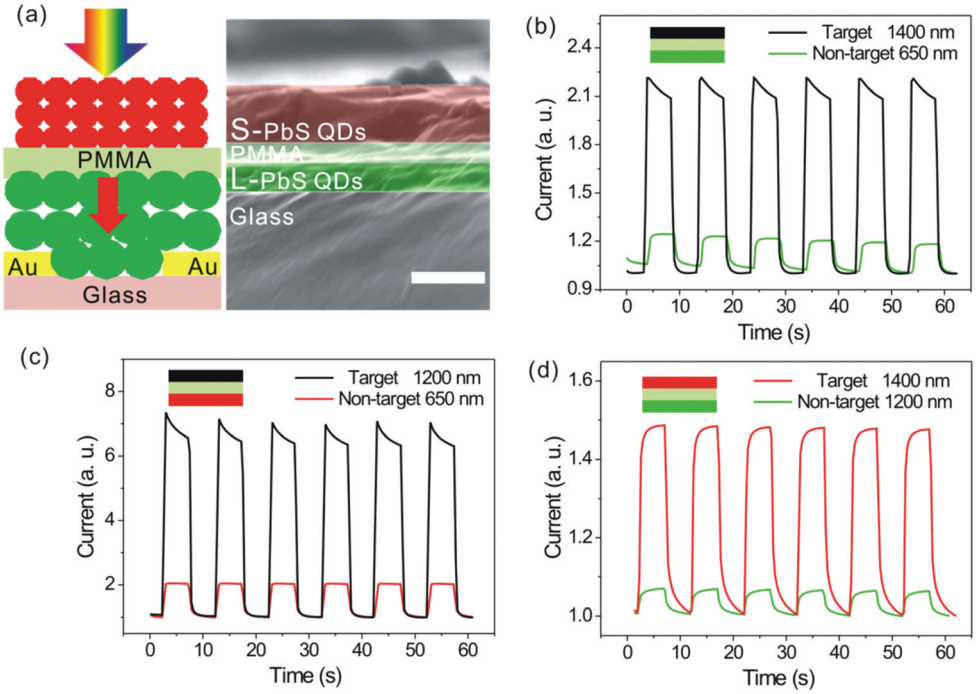

Fig. 5 Performances of S-QD/L-QD ss-PDs. (a) Schematic device structure of the glass/L-QD/PMMA/S-QD ss-PDs (left) and cross-section SEM image (right). The scale bar was 500 nm. (b–d) Input-wavelength dependent *I*–*t* curves of 780 nm/1390 nm (b), 780 nm/1060 nm (c) and 1060 nm/1390 nm (d) ss-PDs under the illumination of target and non-target lights. Insets of b–d show the stacking layers of the device compositions in different colors. The black, red and green rectangles denote the780 nm QDs, 1060 nm QDs and 1390 nm QDs, respectively. All the measurements utilized 20 μW cm^{-2} power intensity and 10 V bias voltage.

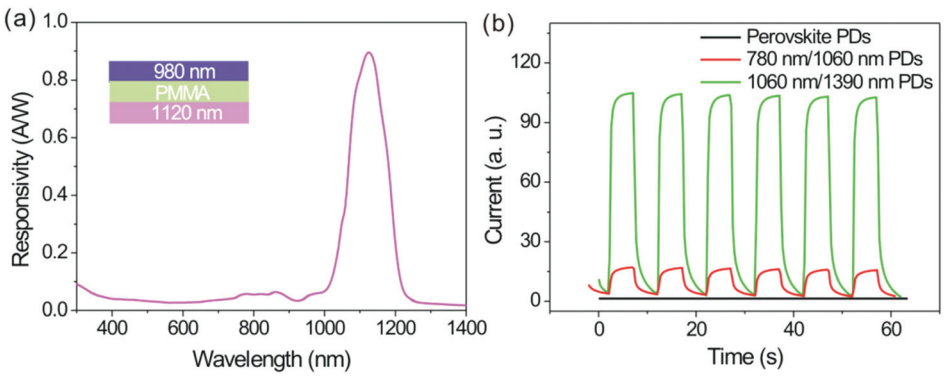

Fig. 6 (a) Narrow response range of 980 nm/1120 nm ss-PDs from full spectra scanning. (b) *I*–*t* responses of perovskite (black), 780 nm/1060 nm (red) and 1060 nm/1390 nm (green) under 1200 nm LED light illumination. The power density and bias voltage were kept at 20 μW cm^{-2} and 10 V, respectively.

a single-crystal of mixed-halide perovskite alloy with the crystal thickness ~1 mm and achieved a narrow spectral response with its FWHM <20 nm by surface-charge recombination.[20] Notably, some defects and impurities in the crystal surface lead to a high rate of charge trapping and recombination[29] thus narrowing the response range. Zhang *et al.* fabricated the wavelength selective metal–semiconductor–metal PDs based on the (Mg, Zn)O-heterostructure and obtained a narrow FWHM of only 7 nm.[17] The devices structure, absorption edge, FWHM and mechanism of the above mentioned devices are summarized in Table 1.

Though they both could get the narrow band PDs by adjusting the halide fraction of the perovskite, yet the maximum wavelength of perovskite they could obtain was about 800 nm. All the OTP based studies can't extend their applications in IR. Furthermore, a hybrid perovskite has poor stability in air. In contrast, PbS QDs can remain stable in air for a long time and hold a large absorption cross section in IR. Furthermore, the

Table 1 A summary of the device structure, absorption edge, FWHM and mechanism of the devices in recent reports

Device structure	Absorption edge (nm)	FWHM (nm)	Mechanism
S-PbS/L-PbS (this work)	980–1120	~100	Filtering
OTP single-crystal PDs[20]	550–600	<20	Surface-charge recombination
OTP PDs mixed with dyes[28]	600–700	<80	Charge collection narrowing
$Mg_yZn_{1-y}O/Mg_xZn_{1-x}O$[17]	325–370	7	(Zn, Mg)O-heterostructure

QD-size-dependent response promises to obtain a series of spectra-selective devices with different response spectra. And it can be conveniently implemented by QD size tuning. The fabrication process was easy, time saving and cheap. The challenges for the present QD based ss-PDs were their large FWHM of response and low response speeds, and the device performance optimization and potential investigation will be developed in further work.

Demos for identifying an unknown light source

The developed ss-PDs were preliminarily applied for identifying an unknown light. Fig. 6b shows the *I–t* response to an unknown light (1200 nm monochromatic light). The light was sequentially tested by OTP PDs, 780 nm/1060 nm ss-PDs and 1060 nm/1390 nm ss-PDs with the same illumination intensity (20 μW/cm^2) and bias (10 V). The selectivity ratio of 1060 nm/1390 nm ss-PDs was 400 times that of perovskite PDs and 10 times that of 780 nm/1060 nm ss-PDs. Therefore, the input light was located at the detection range of 1060 nm/1390 nm ss-PDs (1140–1480 nm). It was expected that the detection range of ss-PDs could be further narrowed by the optimized tuning of the QD size and device engineering. The narrow response range and convenient tuning capabilities enabled the QD based ss-PDs to be widely applied in special application fields such as spectroscopy, confidential communications, surveillance and so on.

Conclusions

In summary, we have systematically demonstrated the ss-PDs by utilizing the semiconductor's "filter" absorption characteristics and QD quantum size effect. A series of PD demos were fabricated and the spectra-selective detection capability was demonstrated. The OTP/QD ss-PDs could tailor the detection range from 800 nm to the onset absorption wavelength of the bottom QD layer. And the full QD based S-QD/L-QD ss-PDs could conveniently tune the QD size to meet the required detection range. The selectivity factor and detectivity ratio of all the ss-PDs can reach more than one order higher than the non-target light excited signal. From full spectrum scanning, the spectra-selective detection of 980 nm/1120 nm ss-PDs was narrowed in the 1000–1200 nm range. The developed ss-PDs was combined together to preliminarily identify an unknown light (1200 nm) and successfully limited it to the 1140 nm–1480 nm range. The high spectra-selective potential and convenient tuning detection range promise the present ss-PDs to be widely applied in future artificial recognition, artificial intelligence, communications and surveillance system.

Experimental section

Synthesis of PbS QDs

The synthesis has been previously published by Hines.[30] The main procedure for 980 nm QDs could be described as follows: 0.45 g lead(II) oxide, 1.5 mL oleic acid and 20 mL 1-octadecane (ODE) were put in a three neck flask. After that, the flask was heated at 90 °C for 16 h under vacuum conditions with vigorous stirring until the solution became clear. Thirdly, the flask was injected with 0.14 mL bis(trimethylsilyl) sulfide once the temperature reached 120 °C. The reaction was carried out for 5 min to obtain the QDs. Products were precipitated by acetone and re-dispersed in toluene three times to prepare 50 mg per mL octane solution ready for device fabrication. PbS QDs with other absorption peaks can be achieved by changing the ratio of the Pb and S precursor and injecting temperature.

Perovskite film fabrication

The perovskite film was synthesized by a two-step method. Firstly, the glass/QD/PMMA substrates were spin-coated with 1 mol per L PbI_2 dimethyl sulfoxide (DMSO) solution at 4000 rpm for 30 s. The spin-coating was repeated until the film thickness reached 300 nm. After that, the PbI_2 film was soaked in CH_3NH_3I isopropanol solution (10 mg mL^{-1}) for 10 min. Finally, the film was rinsed with isopropanol and baked at 75 °C for 15 min to obtain the final perovskite film.

Device fabrication

The Au electrodes were pre-patterned on the glasses by thermal evaporation assisted by shadow mask (15 mm × 0.2 mm for channel). The bottom PbS QD film was deposited by layer by layer spin-coating the PbS QDs octane solution at 2500 rpm for 30 s to reach the required thickness. The solid ligand exchange was carried out by dropping 10% (v/v in methanol) 3-mercaptopropionic acid (MPA) for two times. Then the film was rinsed for 3 times with methanol to remove the residual MPA. Finally, the devices were annealed at 90 °C for 10 min inside a fume hood. The interlayer PMMA was spin-coated the PMMA acetone solution (60 mg mL^{-1}) for 20 layers. The top layer of the perovskite film or QD film was deposited as the same as the aforementioned perovskite or QD film fabrication process.

Material characterization and device measurements

The obtained materials were characterized by UV-Vis absorption spectra (Cary, Lambda 950), X-ray diffraction (XRD, XRD-7000S/L), high-resolution transmission electron microscopy (HRTEM, Tecnai G^2 20 U-Twin), scanning electron microscope (NOVA NANOSEM 450). Performances of PDs were measured using a probe station connected to an Agilent B1500A semiconductor characterization system. The device was further covered with an aluminum cap to provide optical and electromagnetic shielding. Illumination was generated from different light-emitting diodes with different absorption peaks controlled by a functional generator (Agilent 33210A). Light intensity was calibrated using a Silicon PD (Newport 818-UV).

Acknowledgements

This work was financially supported by the National Natural Science Foundation of China (61306137), the Research Fund for the Doctoral Program of Higher Education (20130142120075). The authors also thank the Testing Center of Huazhong University of Science and Technology (HUST) and the Wuhan National Laboratory for Optoelectronics (WNLO) for facility access.

References

1 Z. J. Ning, Y. Ren, S. Hoogland, O. Voznyy, L. Levina, P. Stadler, X. Z. Lan, D. Zhitomirsky and E. H. Sargent, *Adv. Mater.*, 2012, **24**, 6295–6299.
2 Y. X. Yang, Y. Zheng, W. R. Cao, A. Titov, J. Hyvonen, J. R. Manders, J. G. Xue, P. H. Holloway and L. Qian, *Nat. Photonics*, 2015, **9**, 259–266.
3 V. Klimov, A. Mikhailovsky, S. Xu, A. Malko, J. Hollingsworth, C. Leatherdale, H.-J. Eisler and M. Bawendi, *Science*, 2000, **290**, 314–317.
4 A. Woolf, T. Puchtler, I. Aharonovich, T. Zhu, N. Niu, D. Wang, R. Oliver and E. L. Hu, *Proc. Natl. Acad. Sci. U. S. A.*, 2014, **111**, 14042–14046.
5 G. Konstantatos and E. H. Sargent, *Proc. IEEE*, 2009, **97**, 1666–1683.
6 F. W. Wise, *Acc. Chem. Res.*, 2000, **33**, 773–780.
7 Y. L. Wu, C. S. Lim, S. Fu, A. I. Y. Tok, H. M. Lau, F. Y. C. Boey and X. T. Zeng, *Nanotechnology*, 2007, **18**, 215604.
8 X. Cheng, S. B. Lowe, P. J. Reece and J. J. Gooding, *Chem. Soc. Rev.*, 2014, **43**, 2680–2700.
9 J. Chang, Y. Kuga, I. Mora-Sero, T. Toyoda, Y. Ogomi, S. Hayase, J. Bisquert and Q. Shen, *Nanoscale*, 2015, **7**, 5446–5456.
10 W. L. Ma, J. M. Luther, H. M. Zheng, Y. Wu and A. P. Alivisatos, *Nano Lett.*, 2009, **9**, 1699–1703.
11 J. Tang, K. W. Kemp, S. Hoogland, K. S. Jeong, H. Liu, L. Levina, M. Furukawa, X. Wang, R. Debnath, D. Cha, K. W. Chou, A. Fischer, A. Amassian, J. B. Asbury and E. H. Sargent, *Nat. Mater.*, 2011, **10**, 765–771.
12 J. P. Clifford, G. Konstantatos, K. W. Johnston, S. Hoogland, L. Levina and E. H. Sargent, *Nat. Nanotechnol.*, 2009, **4**, 40–44.
13 G. H. Kim, F. P. Garcia de Arquer, Y. J. Yoon, X. Lan, M. Liu, O. Voznyy, Z. Yang, F. Fan, A. H. Ip, P. Kanjanaboos, S. Hoogland, J. Y. Kim and E. H. Sargent, *Nano Lett.*, 2015, **15**, 7691–7696.
14 X. Lan, O. Voznyy, A. Kiani, F. P. García de Arquer, A. S. Abbas, G. H. Kim, M. Liu, Z. Yang, G. Walters and J. Xu, *Adv. Mater.*, 2016, **28**, 299–304.
15 G. Konstantatos, I. Howard, A. Fischer, S. Hoogland, J. Clifford, E. Klem, L. Levina and E. H. Sargent, *Nature*, 2006, **442**, 180–183.
16 E. Przeździecka, A. Wierzbicka, P. Dłużewski, M. Stachowicz, R. Jakieła, K. Gościński, M. A. Pietrzyk, K. Kopalko and A. Kozanecki, *Phys. Status Solidi A*, 2014, **211**, 2072–2077.
17 Z. Zhang, H. von Wenckstern, M. Schmidt and M. Grundmann, *Appl. Phys. Lett.*, 2011, **99**, 083502.
18 P.-N. Ni, C.-X. Shan, S.-P. Wang, X.-Y. Liu and D.-Z. Shen, *J. Mater. Chem. C*, 2013, **1**, 4445–4449.
19 P. Ren, W. Hu, Q. Zhang, X. Zhu, X. Zhuang, L. Ma, X. Fan, H. Zhou, L. Liao, X. Duan and A. Pan, *Adv. Mater.*, 2014, **26**, 7444–7449.
20 Y. Fang, Q. Dong, Y. Shao, Y. Yuan and J. Huang, *Nat. Photonics*, 2015, **9**, 679–686.
21 G. C. Xing, N. Mathews, S. Y. Sun, S. S. Lim, Y. M. Lam, M. Gratzel, S. Mhaisalkar and T. C. Sum, *Science*, 2013, **342**, 344–347.
22 B. R. Sutherland, S. Hoogland, M. M. Adachi, C. T. O. Wong and E. H. Sargent, *ACS Nano*, 2014, **8**, 10947–10952.
23 I. Moreels, K. Lambert, D. Smeets, D. D. Muynck, T. Nollet, J. C. Martins, F. Vanhaecke, A. Vantomme, C. Delerue, G. Allan and Z. Hens, *ACS Nano*, 2009, **3**, 3023–3030.
24 F. Fan, P. Kanjanaboos, M. Saravanapavanantham, E. Beauregard, G. Ingram, E. Yassitepe, M. M. Adachi, O. Voznyy, A. K. Johnston and G. Walters, *Nano Lett.*, 2015, **15**, 4611–4615.
25 L. Gao, D. D. Dong, J. G. He, K. K. Qiao, F. R. Cao, M. Li, H. Liu, Y. B. Cheng, J. Tang and H. S. Song, *Appl. Phys. Lett.*, 2014, **105**, 153702.
26 L. Hu, J. Peng, W. W. Wang, Z. Xia, J. Y. Yuan, J. L. Lu, X. D. Huang, W. L. Ma, H. B. Song, W. Chen, Y. B. Cheng and J. Tang, *ACS Photonics*, 2014, **1**, 547–553.
27 J. Burschka, N. Pellet, S. J. Moon, R. Humphry-Baker, P. Gao, M. K. Nazeeruddin and M. Gratzel, *Nature*, 2013, **499**, 316–319.
28 Q. Lin, A. Armin, P. L. Burn and P. Meredith, *Nat. Photonics*, 2015, **9**, 687–694.
29 M. B. Johnston, *Nat. Photonics*, 2015, **9**, 634–636.
30 M. A. Hines and G. D. Scholes, *Adv. Mater.*, 2003, **15**, 1844–1849.